Multimode – Coreless – Multimode Fiber-based Sensors: Theoretical and Experimental Study

Noé San Fabián, Abián B. Socorro-Leránoz*, Ignacio Del Villar, Silvia Díaz, Ignacio R. Matías, *Senior Member, IEEE*

***Abstract*—This paper presents a complete study on the spectral behavior of a multimode-coreless-multimode fiber-optic structure, as well as its application as a refractometer and liquid level sensor. The combination of two standard multimode fibers fused to a coreless fiber segment allows generating narrow interferometric bands in the optical spectrum, whose sensitivity can be improved by an adequate selection of the dimensions of the device (the coreless segment length and the diameter of the sensing area). A second way to improve the performance of the device is to deposit a thin-film of SnO_2, which allows increasing the sensitivity up to 314 nm/RIU. This widens the number of applications where this structure can be used. As an example, a liquid level sensor with 0.73 nm/mm sensitivity is presented.**

***Index Terms*— Optical fiber sensor, refractive index, multimode-coreless-multimode (MCM), interferometer, refractometer, water level sensor.**

I. Introduction

NOWADAYS there is a trend towards monitoring the world around us. Consequently, sensors are becoming more and more important. More specifically, optical sensors offer high sensitivity, electromagnetic immunity, reduced weight, cost and size, and the option to work in a distributed sensing network. Although their commercial presence is not as widespread as it is the case of electronic sensors, the progress made in the field of optical sensors is opening the door to new opportunities and the use of this kind of sensors is more common over time. In this sense, fiber-optics has experienced an increasing interest and relevance as an adequate technology that combines the advantages of optical sensors in reduced-size and cost effective devices [1].

Currently there are many different types of fiber-optic sensing structures. Among them, fiber Bragg gratings (FBGs) [2], long-period fiber gratings (LPFGs) [3], resonance-based sensors [4-5] and interferometers. Regarding the latter group, interferometers, a wide variety of structures has been developed: single-mode – multimode – single-mode (SMS) both in transmission and reflection versions [6-8], capillary and heterogeneous structures [9-10] or the structure studied in this paper: multimode – coreless – multimode (MCM) [11]. Most of these interferometric structures share a similar design and own the advantages of their easiness when being manufactured and the low cost of the structures. Additionally, they provide high-resolution measurements due to their capability of developing prominent attenuation/transmission bands. Moreover, although they are structures with a low sensitivity, it is possible to improve this magnitude by combining the reduction of the diameter with the deposition of a thin-film whose refractive index is higher than the refractive index of the optical fiber [6].

Among the interferometers mentioned, probably the MCM design is one of the simplest structures, since the fact of using standard fibers, as in this case, normally decreases the cost of the device. This supposes an advantage if compared to other structures such as certain complex Fabry-Perot-based interferometers [12], where it is necessary to create air bubbles and/or grooving one of the fibers to obtain deep and high resolution interferometric bands but a lack of sensitivity enhancement. In addition, the MCM structure is suitable to insert more light from the coreless segment to the collecting multimode fiber, since the diameter of a multimode fiber (MMF) is wider than the diameter of a single-mode fiber (SMF).

However, though there exist interesting works on the MCM structure where the influence of the coreless segment on the performance of the device is analyzed [11], or where the coupling to localized surface plasmon resonances (LSPRs) is used to develop a biosensor in the visible wavelength range [13], a more detailed study is required that relates the attenuation and transmission bands in the optical spectrum to the self-image (SI) band, as it has been done with the SMS structure [11,14]. Moreover, in addition to the coreless segment length it is necessary to study the influence of the cladding diameter and the effect of depositing a nanocoating, which in [6] has led to an important sensitivity improvement. As a proof of concept for the performance of the device, the devices will be tested against refractive index, which is one of the most typical applications of fiber-optic sensors and it is typically used as an assessment tool for determining the further performance when used as chemical or biological sensor [15,16]. After that, and thanks to the conclusions extracted from the refractometric sensor, a more specific application consisting of an optimized liquid level sensor will

Manuscript received on Ago 8, 2018; This work has been supported by the Spanish Ministry of Economy and Competitiveness (TEC2016-78047-R).

The authors are with the Institute of Smart Cities and with the Department of Electrical, Electronic and Communication Engineering, Public University of Navarre, 31006 Pamplona, Navarre, Spain (e-mail: *ab.socorro@unavarra.es, ignacio.delvillar@unavarra.es, silvia.diaz@unavarra.es, natxo@unavarra.es).

be presented.

The outline of this contribution is the following: the second section will present the optical set-ups and the chemical materials used along the corresponding experiments. Then, the spectral behavior of the MCM structure will be analyzed in section 3 as a function of the coreless segment length (CSL) and the sensing area diameter. The performance of the device as a refractometer and a liquid level sensor will be tested in section. Finally, some conclusions on the use of this simple interferometer as an optical sensing platform will be extracted.

II. Materials and Experimental Set-up

As commented in the introduction and depicted in Fig. 1a, an MCM structure consists of two standard multimode fiber-optic pigtails (in this case from Telnet Redes Inteligentes S.A) fused to both sides of a coreless optical fiber segment of length *L* (POFC Inc.). The total diameter of the manufactured waveguide is 125 microns. In this case, an ASBN-W-High power series white light source from Spectral Products Inc. launched the light inside the waveguide and either an HR-4000 or a NIR 512 spectrometer from OceanOptics Inc. were used in order to receive the light in a broadband spectrum ranging from 400 to 1700 nm. The case under analysis, a 60 mm coreless segment, leads to the creation of a self-image band at the end of the coreless segment, as it is shown in the optical intensity diagram obtained with FIMMWAVE® and presented in Fig. 1a.

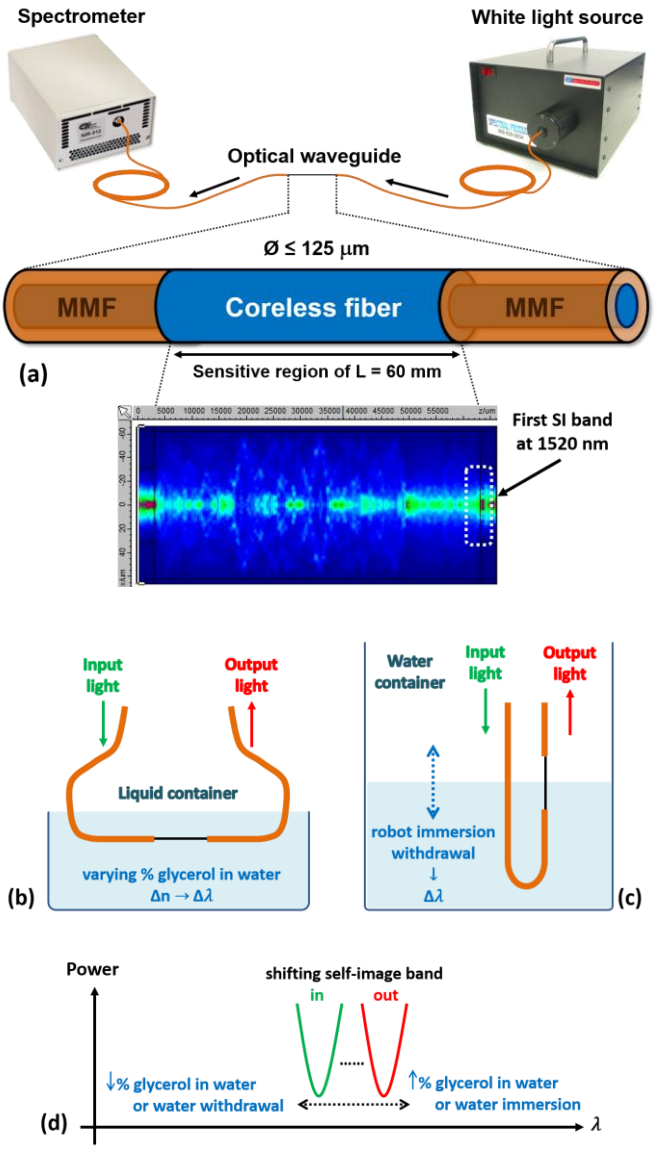

Fig. 1. (a) Experimental set-up used for characterization and detection using the MCM structure. The optical intensity distribution on the x–z plane at a wavelength of 1520 nm for an MCM structure with a coreless segment of 60 μm is shown. (b) and (c) are schematics of both refractometric and liquid level measurements, indicating the wavelength shift as a function of the varying variable that makes possible the detection. These variations are reflected as either blue or red shifts, as indicated in (d).

Regarding the materials used in the experiments, in order to detect surrounding refractive index (SRI) changes outside the waveguide, several solutions of glycerol (Sigma Aldrich Inc.) in ultrapure water were prepared in order to cover a range from 0 to 60% v/v concentration, what means a refractive index range from 1.33 to 1.40 refractive index units (RIU). Refractometric measurements were taken in transmission configuration (see Fig. 1b), and the results were corroborated with FIMMWAVE®. The expected evolution of the interferometric bands is schematically represented in Fig. 1d.

In order to test the spectral behavior and the sensitivity of these structures, several devices with CSLs = 15, 20, 25, 30, 40, 50, 60 and 70 mm were manufactured. Some of them were subjected to diameter reduction. This was made by performing an etching process consisting of immersing the MCM structures in 40% v/v hydrofluoric acid, following the instructions indicated in [6]. Moreover, some sensors were subjected to a sputtering process of tin-oxide (SnO_2) with deposition parameters: Argon pressure = 0.09 mbar and polarization current = 90 mA. The deposition induces a red-shift of the spectrum that leads to a higher sensitivity [14]. However, it is important to avoid depositing a thin-film where the mode transition takes place, since a non-desired lossy mode resonance can fade the necessary attenuation bands shown in Fig. 2, as it has been demonstrated in previous works [14-15]. According to this, it was checked that a deposition time of 45-60 seconds allows obtaining a good sensitivity without reaching the mode transition region.

The measurements of the water level were performed by immersing the sensors in ultrapure water using an ND-Dipper robot by Nadetech Innovations S.L, as shown in Fig. 1c. In this way, the control of the immersion – withdrawal process ensured to make accurate displacements, whose effect on the wavelength shift is also described in Fig. 1d.

III. Spectral Analysis as a Function of the MCM Dimensional Parameters

In an MCM structure, similarly to the SMS structure, the self-imaging (SI) distance pertains to where the light field at the input of the coreless segment is replicated, in both amplitude and phase, on the output of the coreless segment for a specific wavelength [17]. According to [18], the SI distance can be obtained when no restrictions in the excitation of

modes in the MMF segment are applied, at a distance L that obeys to this general expression:

$$L = \frac{4pnD^2}{\lambda} \; ; \; p = 1,2,3,\ldots \quad (1)$$

where D and n are the waveguide diameter and refractive index, respectively, and λ is the operational wavelength. The integer factor p denotes the periodic nature of the imaging along the multimode waveguide [18]. Consequently, an MCM structure of length L that satisfies expression (1), will present a transmission band centered at a wavelength λ, which will be called henceforward self-image band or SI band.

Hereafter, a study on the variation of two variables of expression (1) will be performed, the coreless segment length L and the waveguide diameter D, and on their influence on the sensitivity of the SI band.

A. *Varying the MCM coreless segment length*

In Fig. 2a, and according to by Jung et al. [11], different MCM structures of lengths ranging from 30 to 70 mm were analyzed with the novelty that, in some cases, two bands can be observed. For CSLs = 60 and 70 mm, the attenuation peak is located at 650 and 764 nm respectively, whereas a transmission peak can be observed in the NIR range of both spectra, located at 1293 and 1520 nm respectively.

By applying expression (1) it is easy to observe that the band obtained at 1293 and 1520 nm with CSL 60 mm and 70 mm fits with the wavelength of the first SI band, whereas the other band, located at a shorter wavelengths, is related to half of the SI length. In fact, contrary to the SI band, which is a transmission band, the other band has the form of a dip. This agrees with the fact that for the SI the phase changes of all the modes along the CSL differ by integer multiples of 2π, whereas for half this length the phase changes by integer multiples of π. In view of this, by setting p = 1 in expression (1), a good approximation is obtained to estimate the behavior of the first SI band in the MCM structure of CSL 60 and 70 mm. Moreover, dividing by the obtained wavelength for all MCM structures ranging from 30 to 70 nm, another good approximation is achieved for the dips corresponding to half the length of the SI (see Fig 2b). The supplementary material uploaded with this article (S1) shows a numerical spatial analysis on the field intensity that corroborates this spectral behavior.

All things considered, from a sensing point of view, the main conclusion extracted from this first analysis, is the presence of an attenuation band that can be obtained with shorter CSLs, which is advantageous in terms of reduction of the sensor size. This property will be used during the rest of this work.

B. *Varying the MCM diameter*

Regarding the analysis of the diameter, a video of the optical spectra collected during the etching process is attached in the supplementary material of this work as Visualization 1. A 30 mm-length coreless segment was used in this case to fabricate the MCM structure, leading to an attenuation band located near 1550 nm. A fusion of VIS-NIR spectra was monitored in order to sweep a broadband spectrum from 400 to 1680 nm. It can be observed that the spectrum experiences a blue-shift in wavelength, which agrees with expression (1), where the wavelength is directly proportional to the diameter. In Fig. 3, this effect can also be visualized. The results demonstrate that it is possible to control the location of the attenuation band with the etching process. After 20 minutes of etching, a second transmission band (the SI band) can be visualized, obtaining a spectrum very similar to an MCM with a CSL of 60 mm, although clearly attenuated due to the lower diameter of the structure.

C. *Varying both length and diameter*

In order to complete the analysis, MCM structures with CSLs = 10, 20, 25 and 30 mm were analyzed. The goal was to etch them and try to deduce if there were any substantial changes in the blue-shift rate of the attenuation band, which is related to an enhancement in terms of sensitivity, as indicated in [19] (see Fig. 3).

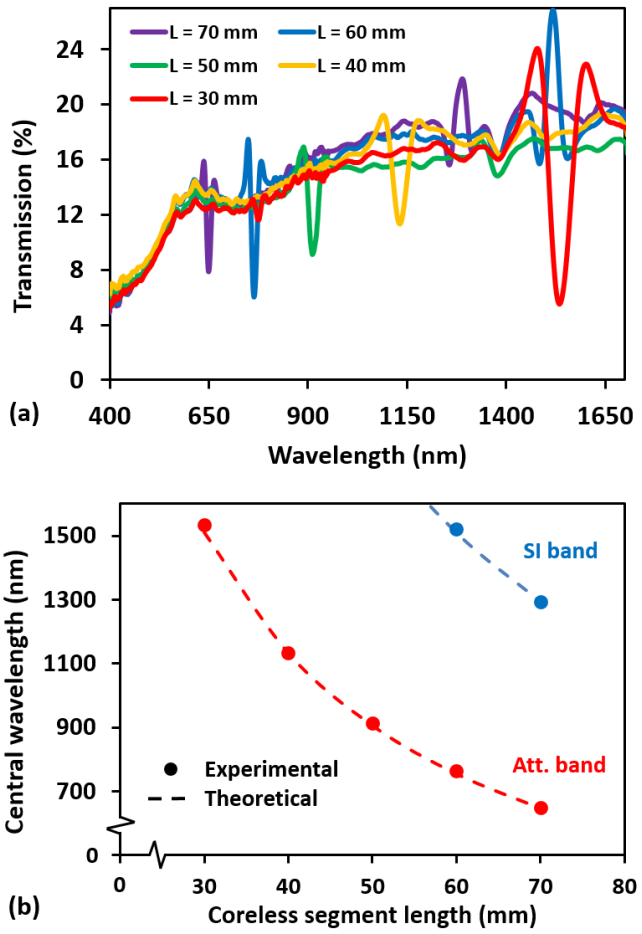

Fig. 2. (a) Spectral evolution of the attenuation bands as a function of the MCM's coreless segment length (CSL). (b) Experimental data and theoretical corroboration of the inverse proportionality between the interferometric bands and the wavelength.

The first consideration to mention on these results is that, when the CSL is reduced, it takes longer to visualize the attenuation band. For instance, in the case of L = 10 mm, this band is obtained after 26 minutes. In the case of L = 20 mm, it is obtained after 9 minutes. For L = 25 mm it takes 5 minutes and for L = 30 mm the band is already located at 1550 nm before starting the etching process.

It can also be observed that there is a high attenuation along the whole spectrum, which is even higher as long as the CSL segment increases. Taking a look to the color bars located at the right side of Fig. 3, it can be observed that in the case of L = 30 mm there is a drastic power loss of around 85% after fusing the coreless segment. On the other hand, after fusing the segment of L = 10 mm, these losses reach 55%. This makes sense for two reasons. The first one is that the CSL segment is a coreless fiber. Consequently, part of the light propagating within the structure escapes as evanescent field. The second is that as the CSL segment increases, the effect of the interferometry is also higher, which contributes to an increase in the overall power loss.

Other considerations have to do with the wavelength shift of the attenuation band as the etching process takes place. At first sight, looking at Fig. 3, there is an apparent parallelism of the attenuation band shifts in all cases. By analyzing the data, it can be observed that in the case of L = 10 mm, the observable shift rate of the attenuation band is 270 nm in 3.33 minutes. In the case of L = 20 mm, there is a wavelength shift of 800 nm in 15 minutes. In the case of L = 25 mm, there is an 800 nm shift in 18 minutes. Finally, in the case of L = 30 mm, there is a 650 nm-shift in 15 minutes. The registered shift in the case of CSL = 10 mm is lower than in the rest of the structures. That is why only the results obtained for MCMs with CSL = 30, 25 and 20 mm are compared, showing 43, 47 and 53 nm/min shift rates respectively. The increase observed as a function of the CSL is because the wavelength shift is monitored when the diameter is smaller for MCMs with a shorter CSL (in Fig. 3b the band shift can be tracked after 10 minutes of etching, whereas in Fig. 3d it is monitored from the beginning). In any case, the improvement of the wavelength shift rate attained if we compare MCMs with 30 and 20 mm is only 18.7%.

Additionally, there are two more aspects to comment regarding etching. One of them is that the attenuation bands obtained at the beginning of the process are drastically vanished while they approach 900 nm, as it can be observed in Visualization 1, due to the lower effect of the interferometries in the VIS-NIR region. Therefore, it is better to work with the attenuation band located within the near-infrared region. The second is that once the structure is reduced to a diameter around 62.5 µm, this means, the standard MMF core diameter, it becomes brittle and the structure is broken. In Fig. 3, three of the four structures analyzed, the MCMs with CSLs 10, 20 and 25 mm, were etched until they broke (the signal suddenly changes to 0) and in all cases the etching lasts about 30-35 minutes. In view that in another publication it was checked that for diameters between 125 and 25 µm the diameter is linearly reduced as a function of the etching time [19], the

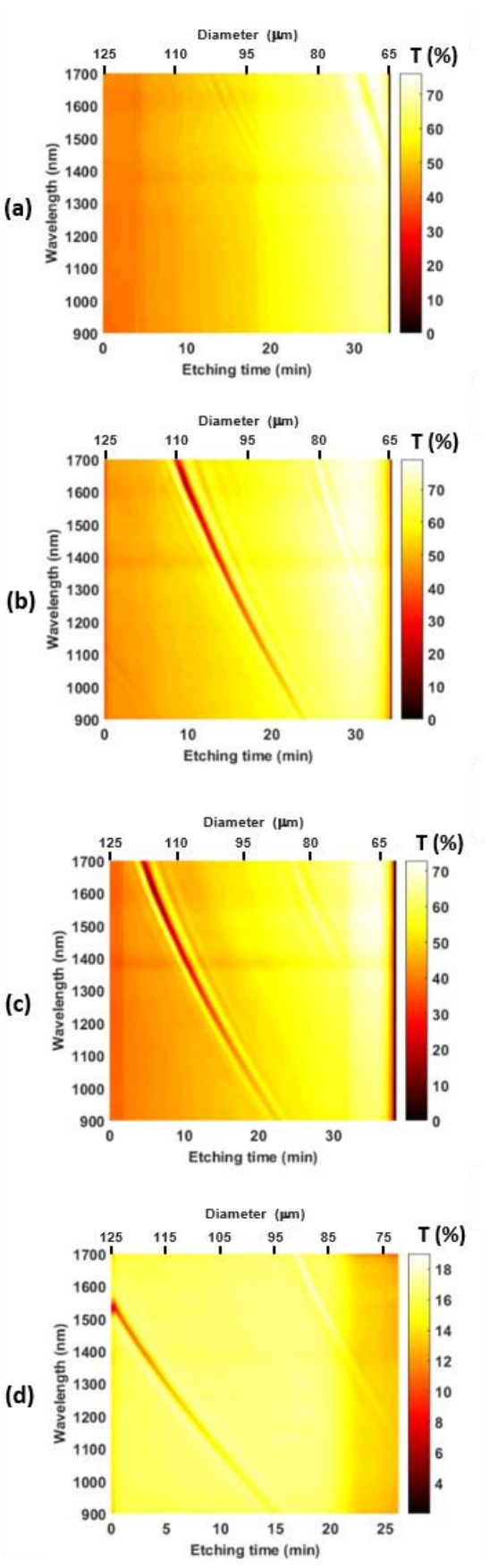

Fig. 3. Etching of several MCM structures using CSLs of (a) 10 mm, (b) 20 mm, (c) 25 mm and (d) 30 mm. Attenuation and transmission bands blue-shift during the etching process.

estimated diameter when the structure breaks is around 65-55 µm. This limitation in the etching process is what explains the slight improvement obtained compared to SMS structure, where diameters below 25 µm can be attained [6,20]. The fact of being capable of reaching lower diameters with the SMS structures is what explains a higher shift rate of the interferometric bands and, therefore, a higher sensitivity to SRI changes, as it will be proved in the next section.

In summary, from an optical structure point of view, it could be said that, provided the transmission or the attenuation bands shown up in the infrared spectrum, it is possible to obtain a sensing platform with good spectral resolution as long as the attenuation band is located above 1500 nm. This can be done by controlling two parameters: the length and the diameter of the device. The length of the device rules the position of the attenuation band and the overall attenuation of the optical spectrum. In general, it is better to work with shorter lengths (less than 35 mm), since the initial transmission losses are reduced and the attenuation band is located at higher wavelengths, what can be beneficious in terms of SRI sensitivity, according to [20].

The second conclusion has to do with the diameter. This parameter can be controlled by etching the structure and permits to accurately adjust the position of the attenuation band when the CSL is short. Moreover, it is possible to obtain a slight improvement in the band shift rate, what can also slightly improve its SRI sensitivity as long as the attenuation band is located near 1500 nm, as mentioned before.

IV. Measurements with MCM-based Sensors

After analyzing the spectral behavior of the bare MCM structure, a characterization of this optical waveguide is presented in the following paragraphs, trying to apply this platform for sensing purposes.

First, the sensitivity to SRI of several MCM structures with CSLs = 30, 40 and 50 mm is analyzed. Fig. 4a reflects the obtained results. The sensor with the highest sensitivity is the one with CSL = 30 mm, with a value of 157 nm/RIU between 1.33 and 1.40 RIU. The MCM sensors with CSL = 40 mm and 50 mm present a sensitivity of 120 nm/RIU and 84 nm/RIU respectively, between 1.33 and 1.40 RIU. As it can be observed, there is an increment in the sensitivity of the structure as a function of the decreasing CSL, which can even suppose doubling the sensitivity with respect to an MCM with CSL = 50 mm. Going back to Fig. 3d, in the case of CSL = 30 mm the attenuation band is located in the third communications window, whereas the structures with CSL = 40 and 50 mm present an attenuation band located below 1500 nm. The explanation of this improvement is that the sensitivity to SRI changes is higher when the attenuation band is located at higher wavelengths. This is something that has already been demonstrated in fiber-optic sensors and, particularly, in interferometry-based fiber-optic sensors [20-22]. The simulations shown in Fig. 4a fit well with the experimental results and they confirm that the sensitivity increases when the attenuation band is located at higher wavelengths. In view of these results, using a long CSL makes no sense in terms of designing a refractometer, which reinforces the first conclusion obtained at the end of section III, where it is stated that it is better to reduce the CSL because otherwise power losses are increased and additionally, the attenuation band can be located at higher wavelengths.

Using the same reasoning, it is possible to deduct the response of the MCM structures after being etched. In this sense, Fig. 4b is presented, which shows the results of the attenuation bands located within the 900 – 1700 nm range. Two analyses can be made here. First, the structures with CSL = 40 and 50 mm keep maintaining the lowest sensitivities, being even lower than without etching. The main reason for this is that, after etching, the attenuation bands are located below 1400 nm, so their sensitivity is clearly lower if compared with their own response without etching.

Fig. 4b also includes the responses of MCMs with CSLs = 15 and 20 mm. They have been etched until their attenuation bands have been centered at 1550 nm in order to make a comparison with the results obtained with the 30 mm-CSL MCM structure. As it can be observed, the device with CSL = 15 mm presents a higher SRI sensitivity (187.5 nm/RIU) than the device with CSL = 20 mm (137.5 nm/RIU). This results is logical since the device with CSL 15 nm presented initially an

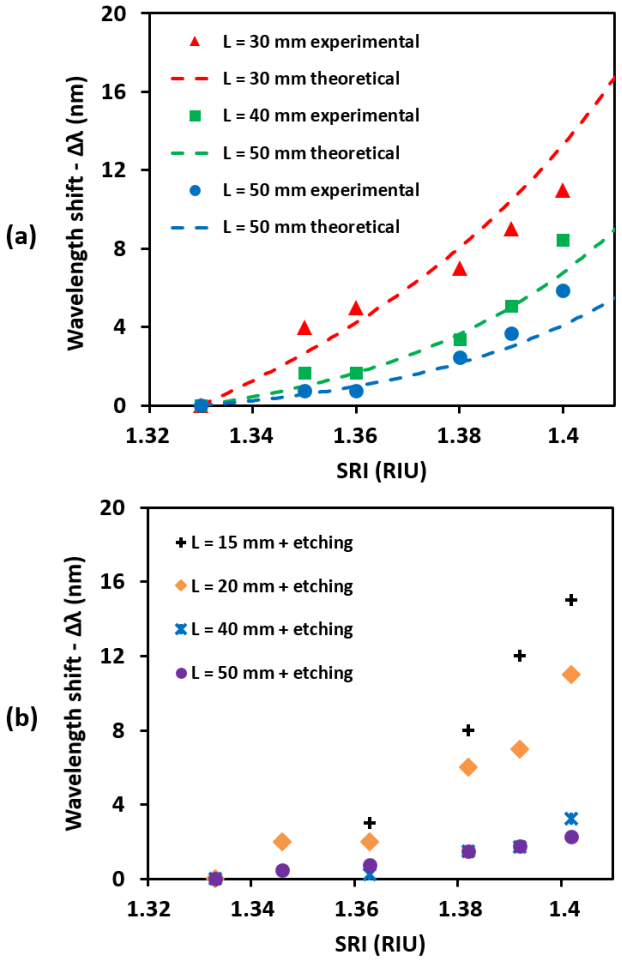

Fig. 4. (a) SRI detection of the different attenuation bands obtained by varying the length of an MCM coreless segment. The dashed lines are the numerical results. (b) Same measurement after etching several structures with different CSLs, in order to test their SRI sensitivity.

attenuation band located at a longer wavelength than the device with CSL= 20 mm. Hence, the deeper etching was applied to position the attenuation band at 1550 nm. The deeper etching means a lower diameter and a higher sensitivity. However, if we compare the results of etched devices with CSL 15 mm and 20 mm with those obtained with the non-etched MCM structure with CSL = 30 mm, there is not a big difference in terms of sensitivity, which confirms the idea presented in section III that the etching is not critical in terms of sensitivity improvement compared to the position of the attenuation band in the optical spectrum. Among the three structures with higher sensitivity, the etched MCM structure with CSL = 15 mm, the etched MCM structure with CSL 20 mm and the non-etched MCM with CSL = 30 mm, the latter is chosen for this purpose because a longer segment allows a wider range in terms of liquid level detection.

In order to test the device, a technique based on a robotic procedure was applied, very similar to that shown in [23]. The obtained sensitivity was 0.33 nm/mm, and presented high stability during the measurements. This is depicted in Fig. 5a, where the response of the sensor to three immersion-withdrawal cycles in water is shown. Every increasing/decreasing step corresponds to sequences of 5 seconds where the robot is stopped to stabilize the measurement. As it can be observed, steps are equally levelled and the structure shows a clear symmetry and repeatability along the whole experiment up to an overall wavelength shift of 10 nm for the 3 cycles analyzed.

Once this bare structure was optimized in terms of dimensions for liquid level measurements, the next step was to obtain an increased sensitivity. As mentioned at the beginning of this contribution, a good way to do that is to deposit a thin-film of higher refractive index than the substrate (i.e. the optical fiber) [6]. In this case, the MCM with CSL = 30 mm was deposited with SnO_2 for 1 minute. After the deposition, the attenuation band was located at 1570 nm and its SRI sensitivity increased from 157 to 346 nm/RIU, what means a 2.2-factor enhancement.

Regarding the water level measurements, the obtained response can be observed in Fig. 5. By comparing Figs. 5a and 5b it is remarkable how the attenuation band of the coated MCM red-shifts up to a factor of 2.2 with respect to the shift obtained without depositing the structure. Also, as in Fig. 5a, the stopping values remain quite well along the three cycles and no apparent hysteresis shows up between upside and downside steps. The bare MCM device with CSL = 30 mm presents a sensitivity of 0.33 nm/mm, whereas the sensitivity enhances to 0.73 nm/mm after the deposition of the thin-film. This remarkable difference can be checked in Fig. 5c, where a quite linear trend is observable in the behavior for both bare and coated sensors.

V. Conclusions

The data shown in this paper demonstrate the spectral behavior of an MCM structure as well as how to improve its sensitivity by either varying its dimensional parameters or depositing a higher refractive index thin-film towards development of sensing applications.

First, the coreless segment length affects the response of the device. Based on the obtained results, by varying the coreless segment length it is possible to tune the central wavelength of either the self-image or the attenuation bands resulting from the mode beatings inside the interferometer. Regarding sensitivity, a better response can be achieved by adjusting the coreless segment length so that the bands are located within the third communications window and this is attained for short segments, which is good in terms of developing compact sensors. Oppositely, the diameter of the waveguide also influences the spectral response, but its contribution performance is low because, unlike in SMS structures, it is not possible to reduce the diameter to values below 50 µm without breaking the structure. Consequently, unetched and short

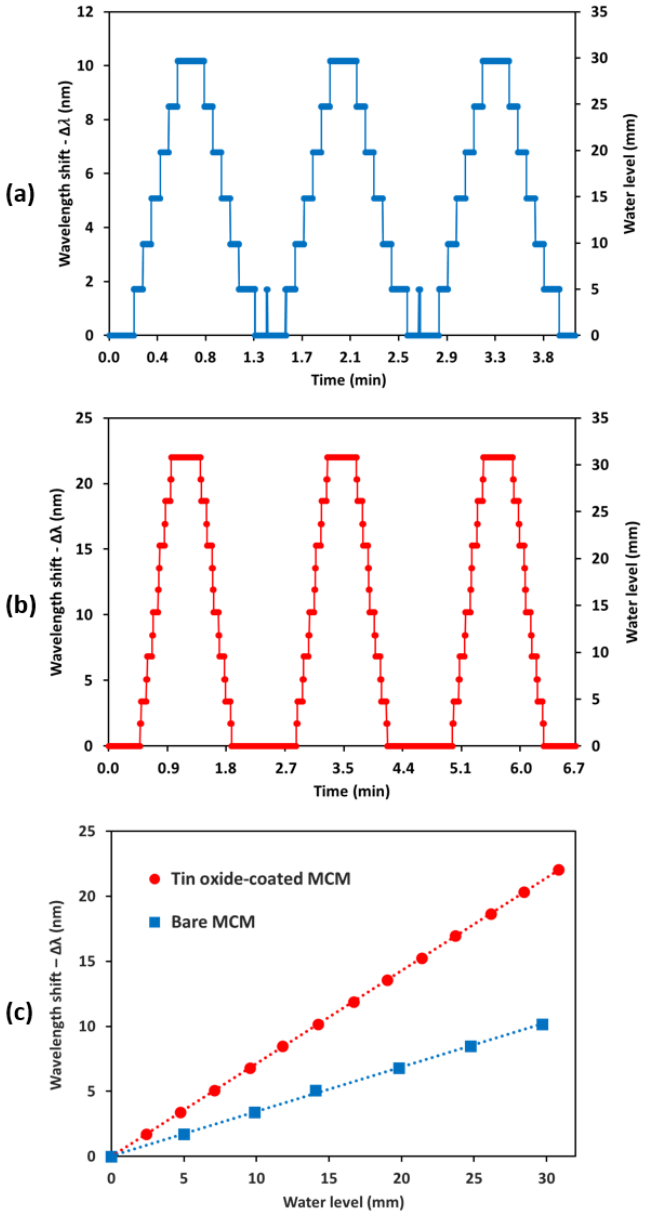

Fig. 5. Experimental evolution of the water level performance for (a) a bare MCM structure with CSL = 30 mm and (b) the same structure coated with a thin-film of tin oxide. (c) Sensitivity comparison between bare and coated sensors.

length MCM structures are the best option in terms of sensing. A third parameter analyzed was the deposition of a thin-film of higher refractive index material than the optical fiber. This strategy has been used in long period gratings and in SMS structures for improving the sensitivity thanks to the mode transition phenomenon, but it was important to check if the same improvement was obtained with the MCM structure. By comparing the same MCM structure with and without coating, it was observed a sensitivity up to 346 nm/RIU after the deposition, what supposed a 2.2 factor enhancement if compared to the bare MCM structure.

As a result, it can be concluded that no diameter reduction, coreless segment length adequate to position the transmission or attenuation bands at long wavelengths where high visibility and sensitivity of the band is attained, and deposition of a high refractive index thin-film are the three main things that must be considered in order to obtain optimized MCM based sensors. As a proof of concept, a liquid level sensor was developed and, according to the results obtained for the refractometer, the sensitivity of the thin-film deposited device multiplied by three the results of the bare structure, while maintaining its mechanical stability and repeatability.

All things considered, the study presented here has proved that a wide variety of parameters can be tuned in the MCM structure towards optimized designs. Moreover, proving that it is possible to apply thin-films with an increased sensitivity opens the path towards the development of other applications such as humidity, chemical, or biological sensors. The main limitation of this structure is that its sensitivity is not very high, but at the same time it is a very simple structure that in the VIS/NIR region can be used with cost-effective sources and detectors.

REFERENCES

[1] T.G. Giallorenzi, J.A. Bucaro, A. Dandridge, G.H. Sigel, J.H. Cole, S.C. Rashleigh, R.G. Priest. "Optical fiber sensor technology". IEEE Transactions on Microwave Theory and Techniques, Vol. MTT-30, No. 4, April 1982.

[2] S. Diaz, N. San Fabian, A.B. Socorro-Leranoz, I.R. Matias. "Temperature sensor using a multiwavelength Erbium-doped fiber ring laser", Journal of Sensors, Vol. 2017, Article ID 8187451, 6 pp.

[3] F. Chiavaioli, P. Biswas, C. Trono, S. Jana, S. Bandyopadhyay, N. Basumallick, A. Giannetti, S. Tombelli, S. Bera, A. Mallick, F. Baldini, "Sol–gel-based titania–silica thin-film overlay for long period fiber grating-based biosensors," Analytical Chemistry, Vol. 87, No. 24 (2015), pp. 12024 – 12031.

[4] I. Del Villar, C.R. Zamarreño, M. Hernáez, F.J. Arregui, I.R. Matias, "Lossy mode resonance generation with indium-tin-oxide-coated optical fibers for sensing applications," Journal of Lightwave Technology, Vol. 28, No. 1 (2010), pp. 111–117.

[5] J. Homola, "Surface plasmon resonance sensors for detection of chemical and biological species", Chemical Reviews, Vol. 108, No. 2 (2008), pp. 462–493.

[6] Y. Cardona-Maya, I. Del Villar, A.B. Socorro, J.M. Corres, I.R. Matias, F. Botero-Cadavid. "Wavelength and phase detection based SMS fiber sensors optimized with etching and nanodeposition". Journal of Lightwave Technology, Vol. 35, No. 17 (2017), pp. 3743-3749.

[7] X. Zhou, K. Chen, X. Mao, W. Peng, Q. Yu. "A reflective fiber-optic refractive index sensor based on multimode interference in a coreless silica fiber". Optics Communications, Vol. 340 (2015), pp. 50-55.

[8] Y. Gong, T. Zhao, Y.J. Rao, Y. Wu, "All-fiber curvature sensor based on multimode interference", IEEE Photonics Technology Letters, Vol. 23, No. 11 (2011), pp. 679-681.

[9] L.H. Chen, T. Li, C.C. Chan, R. Menon, P. Balamurali, M. Shaillender, B. Neu, X.M. Ang, P. Zu, W.C. Wong, K.C. Leong, "Chitosan based fiber-optic Fabry–Perot humidity sensor", Sensors and Actuators B 169 (2012), pp. 167–172.

[10] Y. Luo, L. Xia, C. Yu, W. Li, Q. Sun, Y. Wang, D. Liu, "Multi-parameter optical fiber sensor based on enhanced multimode interference", Optics Communications, Vol. 344 (2015), pp. 120-124.

[11] Y. Jung, S. Kim, D. Lee, K. Oh, "Compact three segmented multimode fiber modal interferometer for high sensitivity refractive-index measurement", Measurement Science and Technology, Vol. 17 (2006), pp. 1129–1133.

[12] Y. Gong, Y. Guo, Y.J. Rao, T. Zhao, Y. Wu, "Fiber-optic Fabry–Pérot sensor based on periodic focusing effect of graded-index multimode fibers", IEEE Photonics Technology Letters, Vol. 22, No. 23 (2010), pp. 1708-1710.

[13] Y.R. Wang, Z.Q. Tou, C.L. Zhao, P.L. So, C.C. Chan, "Localized surface plasmon resonance refractometer based on no-core fiber", Proceedings of SPIE, Vol. 10323, 103232R (2017), doi: 10.1117/12.2263473.

[14] A.B. Socorro, I. Del Villar, J.M. Corres, F.J. Arregui, I.R. Matias, "Sensitivity enhancement in a multimode interference-based SMS fibre structure coated with a thin-film: theoretical and experimental study", In Sensors and Actuators B: Chemical, Vol. 190 (2014), pp. 363-369.

[15] A.B. Socorro-Leranoz, D. Santano, I. Del Villar, I.R. Matias. "Trends in the design of wavelength-based optical fibre biosensors (2008 - 2018)". Biosensors and Bioelectronics (2019) (in press).

[16] C. Caucheteur, T. Guo, J. Albert, "Review of plasmonic fiber optic biochemical sensors: improving the limit of detection", Analytical and Bioanalytical Chemistry, Vol. 407, Issue 14 (2015), pp 3883–3897.

[17] A.B. Socorro, I. Del Villar, J.M. Corres, F.J. Arregui, I.R. Matias, "Mode transition in complex refractive index coated single-mode–multimode–single-mode structure", Optics Express, Vol. 21, No. 10 (2013), pp. 12668 – 12682.

[18] S. Silva, E.G.P. Pachon, M.A.R. Franco, J.G. Hayashi, F.X. Malcata, O. Frazao, P. Jorge, C.M.B. Cordeiro, "Ultrahigh-sensitivity temperature fiber sensor based on multimode interference," Applied Optics, Vol. 51 (2012), pp. 3236–3242.

[19] I. Del Villar, M. Partridge, W.E. Rodriguez, O. Fuentes, A.B. Socorro, S. Diaz, J.M. Corres, S.W. James, R.P. Tatam, "Sensitivity enhancement in low cutoff wavelength long-period fiber gratings by cladding diameter reduction", Sensors 2017, 17(9), 2094, 12 pp.

[20] L.B. Soldano, E.C.M. Pennings, "Optical multi-mode interference devices based on self-imaging: principles and applications", Journal of Lightwave Technology, Vol. 13, No. 4 (1995), pp. 615 – 627.

[21] Y. Chen, Q. Han, T. Liu, X. Lan, H. Xiao, "Optical fiber magnetic field sensor based on single-mode–multimode–single-mode structure and magnetic fluid", Optics Letters, Vol. 38, No. 20 (2013), pp. 3999-4001.

[22] Q. Wu, Y. Semenova, P. Wang, G. Farrell, "High sensitivity SMS fiber structure based refractometer – analysis and experiment", Optics Express, Vol. 19, No 9 (2011), pp. 7937-7944.

[23] O. Fuentes, I. Del Villar, J.R. Vento, A.B. Socorro, E.E. Gallego, J.M. Corres, I.R. Matias, "Increasing the sensitivity of an optic level sensor with a wavelength and phase sensitive single-mode multimode single-mode fiber structure", IEEE Sensors Journal, Vol. 17, No. 17 (2017), pp. 5515 – 5522.